Journal of Power Sources 202 (2012) 92–99

Contents lists available at SciVerse ScienceDirect

Journal of Power Sources

journal homepage: www.elsevier.com/locate/jpowsour

High voltage retainable Ni-saving high nitrogen stainless steel bipolar plates for proton exchange membrane fuel cells: Phenomena and mechanism

Masanobu Kumagai[a,b,1], Seung-Taek Myung[d,*,1], Takuma Ichikawa[c], Hitoshi Yashiro[c], Yasuyuki Katada[a,**]

[a] National Institute for Material Science, 1-2-1 Sengen, Tsukuba, Ibaraki 305-0047, Japan
[b] Taiyo Stainless Spring Co., Ltd., 2-8-6 Shakujiicho, Nerimaku, Tokyo 177-0041, Japan
[c] Department of Chemistry and Bioengineering, Iwate University, 4-3-5 Ueda, Morioka, Iwate 020-8551, Japan
[d] Department of Nano Engineering, Sejong University, Seoul 143-747, South Korea

ARTICLE INFO

Article history:
Received 27 June 2011
Received in revised form 31 October 2011
Accepted 15 November 2011
Available online 25 November 2011

Keywords:
Stainless steel
Bipolar plate
Passive layers
Nitrogen
PEMFC

ABSTRACT

In the present paper, we elucidate the possible reasons for high voltage retention during operation when a Ni-saving high nitrogen stainless steel (hereafter referred as to Ni-saving HNS) was used as bipolar plates for PEMFCs. A typical type 316L was also employed as bipolar plates to compare the cell performance. The Ni-saving HNS bipolar plate adopting cell obviously exhibited better cell performance at various current densities. After 1000 h of cell operation, the tested metallic bipolar plates were analyzed by scanning electron microscopy, inductively coupled plasma-mass spectrometry, X-ray photoelectron spectroscopy, transmission electron microscopy–energy-dispersive X-ray spectroscopy, and transmission electron microscopy–electron energy loss spectroscopy to prove the superiority of the Ni-saving HNS bipolar plates. As a result, the surface state of the bipolar plates exposed to the PEMFCs environment is the critical factor that affects cell performance. Protection of the metal surface mainly with chromium oxide-based surface layer, which was induced from a reaction of N from the Ni-saving HNS and H_2O generating proton, H^+, that lowers local surface pH, was thus substantially effective to retain the voltage upon operation.

1. Introduction

Applications of metallic bipolar plates such as Ti-based alloys [1,2], Al-based alloys [1,3,4], Ni-based alloys [1,5,6], Cu-based alloys [7,8], and stainless steels [2,5,6,9–21] have been examined because of their low cost compared to graphite and because of the miniaturization of proton electrolyte membrane fuel cells (PEMFCs). Among them, considerable attention has been given to austenitic stainless steels because of their superior corrosion resistance, which leads to improved cell performance. In general, there are detrimental factors that deteriorate cell performance. For instance, SO_4^{2-} and F^- ions released from the membrane during cell operation tend to corrode the surface of stainless steel. The voltage drop was also caused by the contamination of membrane electrode assembly (MEA), which is mainly ascribed to the adherence of Ni^{2+} ions. It has known that the nickel ingredient is readily dissolved from the stainless steel bulk (type 316/316L) during cell operation, as reported by Wind et al. [10].

For the reason, we hypothesized that, if the Ni concentration decreased the resulting dissolution of Ni^{2+} would be decreased and it was realized by adopting Ni-saving HNS bipolar plate [21]: the Ni-saving HNS bipolar plate employing cells exhibited very promising cell performance during operation. Although the bipolar plate gave convincing electrochemical results that are sufficient to be commercialized, it is difficult to find out the conclusive reasons affecting the superior performance. This necessitates surface analyses of bipolar plates after a long term operation, since the electrochemical reaction occurs on the surface metallic bipolar plates. In the present study, therefore, we revisit the Ni-saving HNS to understand and to prove the detailed mechanism underlying the enhanced cell performance.

2. Experimental

2.1. Specimen preparation

Commercial-type 316L stainless steel and the Ni-saving HNS were used as the PEMFC bipolar plate materials. Melting tests for

* Corresponding author. Tel.: +82 2 3408 3454; fax: +82 2 3408 3454.
** Corresponding author. Tel: +81 29 859 2112; fax: +81 29 859 2886.
E-mail addresses: smyung@sejong.ac.kr (S.-T. Myung), katada.yasuyuki@nims.go.jp (Y. Katada).
[1] These authors contributed equally to this work.

0378-7753/$ – see front matter © 2011 Elsevier B.V. All rights reserved.
doi:10.1016/j.jpowsour.2011.11.033

Table 1
Chemical compositions of stainless steels (mass%).

	C	Si	S	Mn	Cr	Ni	Mo	N	Fe
Type 316L	0.012	0.50	0.001	0.83	17.32	12.03	2.01	–	Balance
Ni-saving HNS	0.022	–	0.0005	3.09	24.07	3.88	1.94	1.06	Balance

the P-ESR were mainly conducted under 4 MPa in nitrogen gas pressure, AC current of 2000–3000 A, voltage of 27–30 V, and melting rate of 0.5–0.7 kg min^{-1}. FeCrN powders, which were used as a nitrogen source, were packed in stainless steel pipes and then sintered, followed by spot-welding on the surface of the electrode. The flux used was CaF_2, all of which was added to the crucible before the melting test. Metallic calcium wire was also attached to the primary electrode for de-oxidation. The chemical compositions of the specimen are given in Table 1. Stainless steel plates (80 mm × 80 mm × 6 mm) were machined into bipolar plates with a single serpentine flow field, in accordance with the NEDO report by JARI [22]. The surfaces of the bipolar plates were then finished using diamond paste polisher (6 μm) and cleaned ultrasonically in hexane for 15 min.

2.2. Single cell operation

A single cell was assembled that adopted the type 316L stainless steel bipolar plates or the Ni-saving HNS and a commercially available MEA (carbon cloth type gas diffusion layers [GDLs]) with compressive force of 150 N cm^{-2} controlled by a torque wrench. The active electrode area was 50 mm × 50 mm. The single cell was operated at 348 K under ambient pressure. The reactant gases were fully humidified at 343 K. The utilization was 70% for the fuel gas (H_2) and 40% for air with flow rates of 0.124 NLPM and 0.520 NLPM, respectively. The applied current density was 0.5 A cm^{-2} (12.5 A).

2.3. Characterization of bipolar plate surfaces after single cell operation

Surfaces of the type 316L stainless steel and the Ni-saving HNS were observed by SEM (JSM-6060LA, JEOL) at an acceleration voltage of 15 kV. The cross-sectional structure of the type 316L stainless steel and the Ni-saving HNS was analyzed by TEM (HF-2000, Hitachi High-Technologies) with EDS (NORAN System 6, Thermo Scientific) at an acceleration voltage of 200 kV. The specimens for TEM were prepared using a focused ion beam system (FIB, SMI3050MS2, SII NanoTechnology) at an acceleration voltage of 30 kV. The nitrogen soluted in the Ni-saving HNS was traced by TEM (JEM-2010F, JEOL) equipped with an aberration called an EELS (Enfina, Gatan).

2.4. The contamination of MEA

The center of the operated MEA was first cut into a predetermined area (10 mm × 10 mm). The MEA was then disassembled into three parts: anodic and cathodic GDLs and membrane (together with a catalyst, Pt). The components were consequently immersed into aqua regia at room temperature to dissolve the adhered metallic ingredients. The dissolved metallic ions, such as Ni^{2+}, Fe^{2+}, and Cr^{3+}, were analyzed by ICP-MS (ELEMENT2, Thermo Fisher Scientific).

2.5. X-ray analysis

After 1000 h of cell operations, the surfaces of the type 316L stainless steel and the Ni-saving HNS were analyzed by XPS (ULVAC-PHI 5600) with a monochromatic Al-Kα source. The analyzed position was the central part of the bipolar plate. The take-off angle of the emitted photoelectrons was adjusted to 45° with respect to the surface.

3. Results and discussion

3.1. Cell performance

Fig. 1a shows current density versus voltage curves of the type 316L stainless steel and the Ni-saving HNS bipolar plate employing cells after 24 h activation process. For the type 316L stainless steel bipolar plate employing cell, the initial cell voltage was approximately 0.65 V at 0.5 A cm^{-2} (12.5 A). The initial cell voltage for the Ni-saving HNS bipolar plate was approximately 0.67 V at 0.5 A cm^{-2}, which is slightly lower than that of the graphite cell (0.70 V at 0.5 A cm^{-2}). Fig. 1b depicts current density versus voltage curves of the type 316L stainless steel and the Ni-saving HNS bipolar plate employing cell after 1000 h of cell operation. Voltage decay of the type 316L stainless steel bipolar plate cell was approximately 48 mV, whereas that of the Ni-saving HNS cell was approximately 17 mV. The Ni-saving HNS bipolar plate cell obviously shows better voltage retention to 1000 h, the voltage drop in which is close to that of the graphite cell (14 mV) despite the

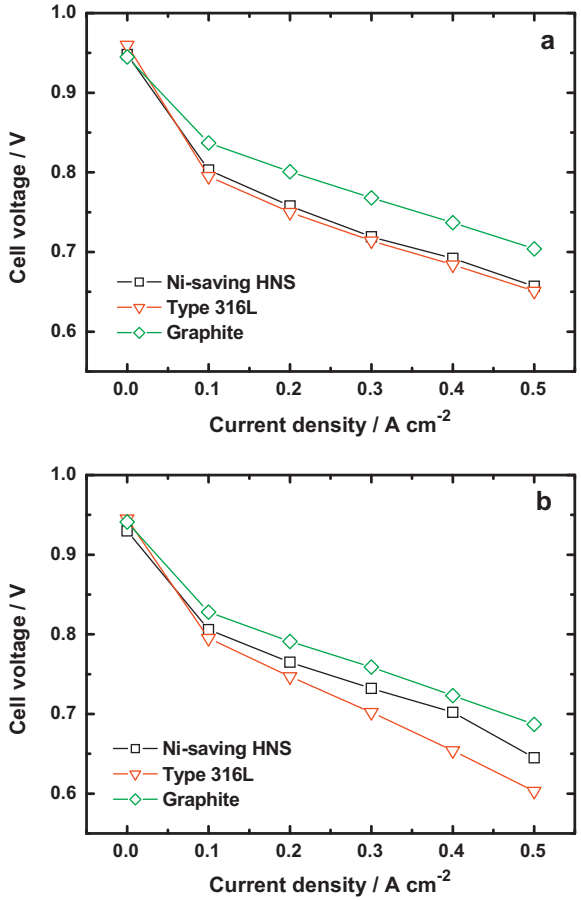

Fig. 1. Comparison of *i–V* characteristics of cells with type 316L stainless steel, Ni-saving HNS, and graphite bipolar plates at (a) initial state and (b) after 1000 h of cell operation.

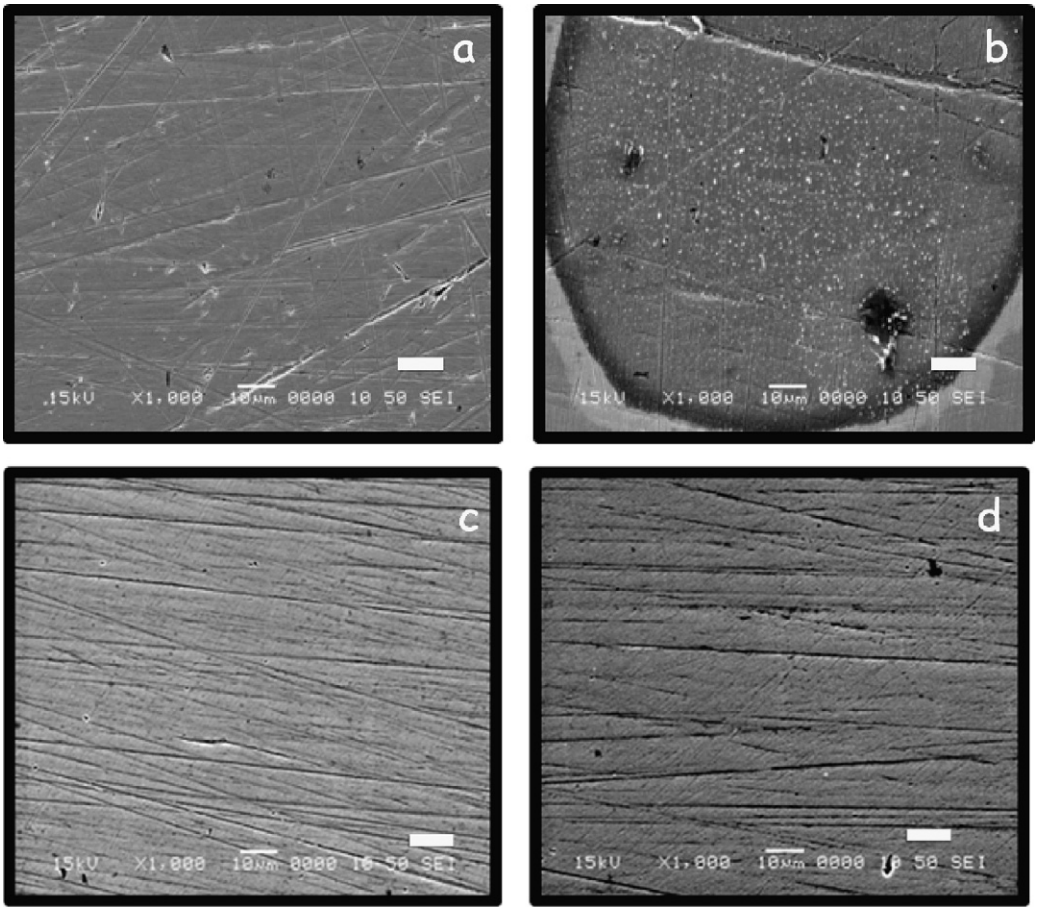

Fig. 2. SEM images of the rib surfaces on (a) anodic side of type 316L stainless steel, (b) cathodic side of type 316L stainless steel, (c) anodic side of Ni-saving HNS, and (d) cathodic side of Ni-saving HNS after 1000 h of cell operation. The scale bar indicates 10 μm.

slightly lower operation voltage. However, this problem can be readily overcome through a surface modification, TiN–SBR hybrid coating [23,24], which gives higher operation voltage comparable to graphite adopting cells because of the reduced ICR achieved by the TiN–SBR hybrid coating.

3.2. Corrosion behavior

After 1000 h of cell operation, the type 316L stainless steel and the Ni-saving HNS bipolar plate employing cells were carefully disassembled and the resulting rib surfaces of the bipolar plates were observed by SEM (Fig. 2). Corrosion traces were not found on the surfaces of the anodic-side bipolar plates for the type 316L stainless steel (Fig. 2a) and the Ni-saving HNS (Fig. 2c). Meanwhile, general/crevice corrosion occurred on the type 316L stainless steel surface for the cathodic side (Fig. 2b). However, the cathodic side of the Ni-saving HNS did not experience such corrosion during the cell operation (Fig. 2d). We previously suggested that the chromium content is the crucial factor to ensure corrosion resistance in the fuel cell operation environment [25]. From this point of view, we speculate that the higher content of chromium in the present Ni-saving HNS seems to be the requisite condition to ensure the corrosion resistance.

3.3. Contamination of membrane and GDL

The corrosion of metal usually accompanies the dissolution of metallic ingredients. In the case of PEMFC, the dissolved metallic components released from the stainless steel bipolar plates can be trapped in the MEA during the cell operation. Given this, each MEA component, membrane (together with catalyst layer) and GDL, was immersed into aqua regia to completely dissolve the existing metallic elements adhered on the membrane and GDLs. Then, the resulting solutions were analyzed by ICP-MS. Fig. 3 shows the results of metallic ions such as Fe^{2+}, Ni^{2+} and Cr^{3+} adhered on the MEA after 1000 h of cell operation. For the membrane part, the amount of Fe^{2+} ions was approximately 0.08 μg cm^{-2} for the type 316L stainless steel bipolar plate employing cell. However, the amount of Fe^{2+} ions was nearly the detection limit for the Ni-saving HNS one. It is reasonable to assume that the membrane was somewhat polluted by Fe^{2+} ions because the type 316L

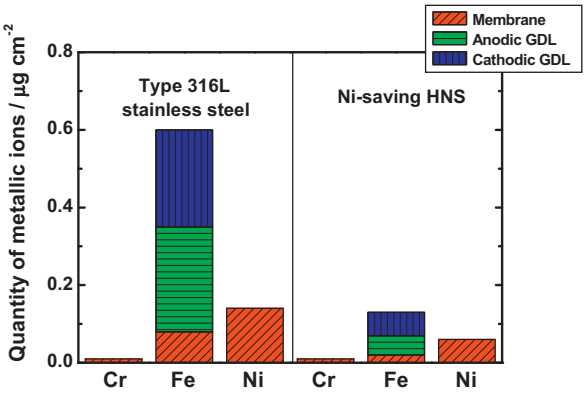

Fig. 3. The amounts of metallic ions fixed to the MEA after 1000 h of cell operation.

stainless steel surface was corroded (Fig. 2b). The amount of Cr^{3+} ions was almost as little as the detection limit for both the type 316L stainless steel and the Ni-saving HNS. The amount of Ni^{2+} ions was 0.14 μg cm^{-2} for the type 316L stainless steel bipolar plate employing cell, whereas the analyzed content was reduced to 0.06 μg cm^{-2} for the Ni-saving HNS one. It is obvious that Ni^{2+} ions adhere or infiltrate into the membrane, but fewer Ni^{2+} ions are found for the Ni-saving HNS. This is a result of the less amount of Ni element (below 4 mass %) in the Ni-saving HNS relative to the 316L stainless steel (*ca.* 12 mass%). It is known that this contamination of the membrane by Ni^{2+} ions affects the degradation of cell performance [10,26]. In this point of view, the Ni-saving HNS, which releases fewer Ni^{2+} ions from the bipolar plate, is beneficial to maintain the integrity of the membrane during cell operation.

For the anodic- and cathodic-side GDLs, the detected amounts of Ni^{2+} and Cr^{3+} ions were negligible for both steels. For the 316L stainless steel, however, the detected content of Fe^{2+} ions was approximately 0.27 μg cm^{-2} for the anodic side and 0.25 μg cm^{-2} for the cathodic side. Surprisingly, the amount of Fe^{2+} ions for the Ni-saving HNS after the operation was reduced as low as 0.05 μg cm^{-2} for the anodic side and 0.06 μg cm^{-2} for the cathodic side GDLs. Because corrosion occurred for the type 316L stainless steel, the amount of Fe^{2+} ions adhered on the GDLs is approximately four- or five-fold greater than the Ni-saving HNS, which did not undergo corrosion. Overall, dissolution of these metallic ions was dramatically suppressed by adopting the Ni-saving HNS bipolar plates. The lower dissolution of metallic ions from the bipolar plates enabled the integrity of the MEA to be maintained and this, in turn, resulted in enhanced cell performance, the voltage retention of which is comparable to the graphite bipolar plate employing cell.

3.4. Surface layers of the steels

Fig. 4 shows the cationic ratio obtained from the chromium oxide versus iron oxide in the passive layer for both steels after 1000 h of cell operations, calculated from the XPS spectra (Fig. 4a, b, d and e) after elimination of the metallic portion. The chromium/iron ratio in the passive layer from the XPS analysis was approximately 51:49 for the as-polished type 316L stainless steel (Fig. 4c) and 37:63 for the Ni-saving HNS (Fig. 4f), meaning that iron oxide constitutes the majority of the passive layer for the Ni-saving HNS.

For the anodic side, the chromium oxide portion increased for both steels, 67:33 (from 51:49) for the type 316L stainless steel (Fig. 4c) and 47:53 (from 37:63) for the Ni-saving HNS (Fig. 4f) after 1000 h of cell operation. As is known, the potential of the anodic bipolar plate (−100 mV vs. SCE) corresponds to the active

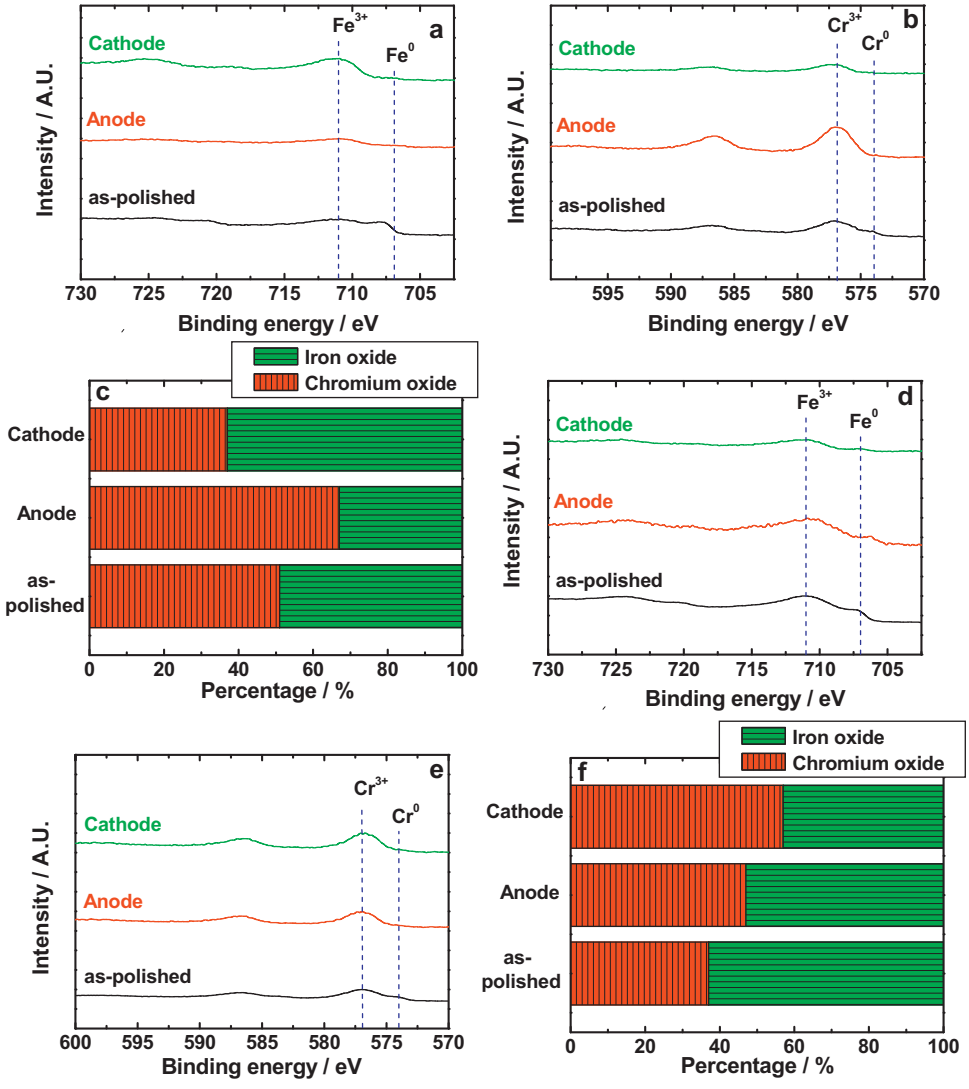

Fig. 4. Cationic ratio of chromium versus iron oxide in the passive film based on XPS analysis for type 316L stainless steel and Ni-saving HNS after 1000 h of cell operation.

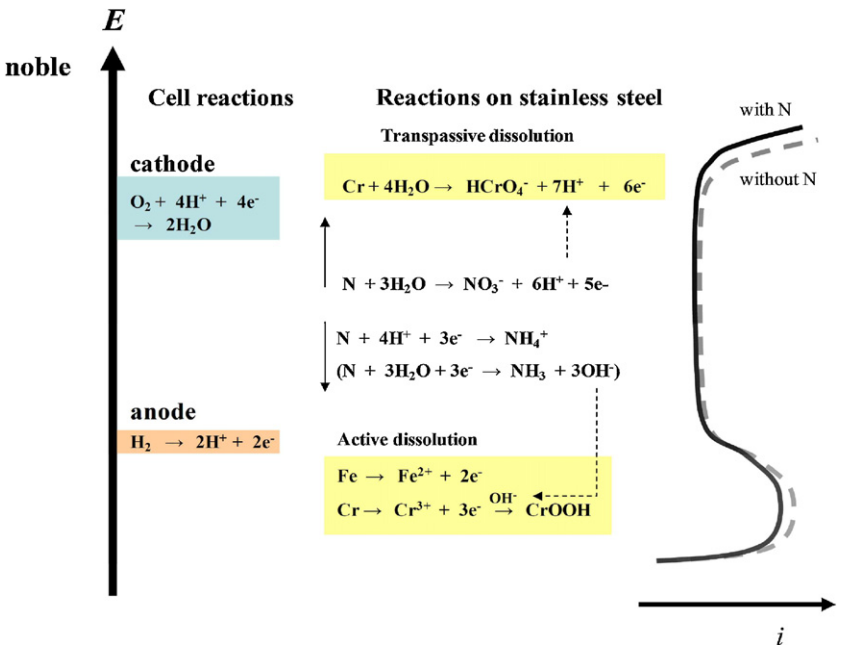

Fig. 5. Schematic of electrochemical reactions on stainless steel.

dissolution region for both steels (see S-Fig. 1). The iron oxide component contained in the passive layer is selectively dissolved in such an acidic condition, so the chromium oxide content becomes the major component to constitute the passive layer. Leckie and Uhlig [27] suggested that the soluted nitrogen follows the reaction in the active region: $N + 4H^+ + 3e^- \rightarrow NH_4^+$. Namely, the soluted nitrogen element is released from the Ni-saving HNS and the nitrogen consequently reacts with H^+ ions in the aqueous solution, resulting in the formation of NH_4^+ ions on the surface of the passive layer. The formed NH_4^+ ions simultaneously cause the pH of the passive layer to increase. Therefore, a relatively large portion of iron oxide (chromium oxide:iron oxide = 47:53) is retained in the passive layer for the Ni-saving HNS. As we previously reported [19], iron oxide in the passive layer is stable in the weak acidic condition (pH ~ 4.3). The XPS results suggest that the resulting pH of the passive layer for the Ni-saving HNS is higher than that of the type 316L stainless steel.

For the cathodic side, the type 316L stainless steel was mainly covered with iron oxide because of the surface corrosion after 1000 h of cell operation (Fig. 4c), whereas the Ni-saving HNS consisted of chromium oxide–enriched passive layer after 1000 h of cell operation (Fig. 4f). The cationic ratio of chromium versus iron in the passive layer approximated to 57:43 for the Ni-saving HNS, indicating that the chromium oxide content increased in the cathodic side relative to the native passive layer. Because the operation environment is situated in a weak acidic condition (pH ~ 4.3 [19]), the passive layer is supposed to be enriched with iron oxide-based passive layer. The reaction potential of the cathodic side is approximately 600 mV (SCE). The potential lays the beginning point of the transpassive dissolution of trivalent chromium to a hexavalent one (see S-Fig. 1). Thus, the selective dissolution of the chromium ingredient at the potential should have led to the formation of the iron oxide–enriched passive layer. Nonetheless, the XPS results indicate the chromium oxide-enriched passive layer. Yashiro et al. [28] reported that nitrogen in the nitrogen-bearing stainless steel was dissolved in a neutral chloride solution at around 550 mV (SCE) prior to the transpassive dissolution of chromium by the following reaction: $N + 3H_2O \rightarrow NO_3^- + 6H^+ + 5e^-$ [28]. The formed H^+ ions thus lead to a decrease in pH in the passive layer, which retards the transpassive dissolution of chromium, and, in turn, facilitates the selective dissolution of iron oxide by the generated H^+ ions. Therefore, the outer surface of the passive layer could be preserved by chromium oxide, which is expected to provide high corrosion resistance. Schematic of electrochemical reactions on stainless steel is summarized in Fig. 5.

3.5. TEM observation of the surface layer

To observe the cross-sectional images of the surface layer directly the operated bipolar plate ribs (see S-Figs. 2a and b) were etched by focused ion beams for the TEM observation. First, we observed undamaged (Fig. 6a) and corroded (Fig. 6c) parts of the operated type 316L stainless steel to compare the passive layer using EDS. As can be seen in Fig. 6a, the passive layer is obviously thicker (~9 nm) for the undamaged part after 1000 h of cell operation than that of the native state, which agrees with XPS results (iron oxide-enriched passive layer: 7–9 nm) of the type 310S stainless steel after 1000 h of cell operation [19]. Generally, the thickness of passive layer on stainless steels is a few nanometers thick. Hamada et al. directly observed [29] that a passive layer thickness of a commercial-type 304 stainless steel was found to be 3 nm using corrected STEM. We consider that the thickened passive layer simultaneously derives an increase in the ICR between the stainless steel bipolar plate and GDLs, and it thus affects steep voltage decay approximately 50 mV (Fig. 1). For the undamaged part, it is suggested that the passive layer is not uniform (Fig. 6a (point 1)). The interface region (Fig. 6a (point 2)) exhibits significantly reduced intensity for oxygen (Fig. 6b (point 2)).

For the damaged part (Fig. 6c), the surface of the stainless steel no longer exhibited a uniform and smooth passive layer. In addition, the passive layer was severely damaged and the sediment of corrosion products is evident on the passive layer (Fig. 6c (point 1)), which is covered with corrosion products such as iron oxide (Fig. 6d (point 1)), which is in agreement with the XPS results (Fig. 4c). The corrosion was progressed not only on the surface of stainless steel but in the depth direction (Fig. 6c (point 2)). The stronger intensity of iron element also supports the formation of corrosion products in the depth direction. Meanwhile, the bulk exhibited a similar EDS spectrum (Fig. 6c (point 3) and d (point 3)), compared with the undamaged bulk (Fig. 6b (point 2)). Therefore, the appearance of

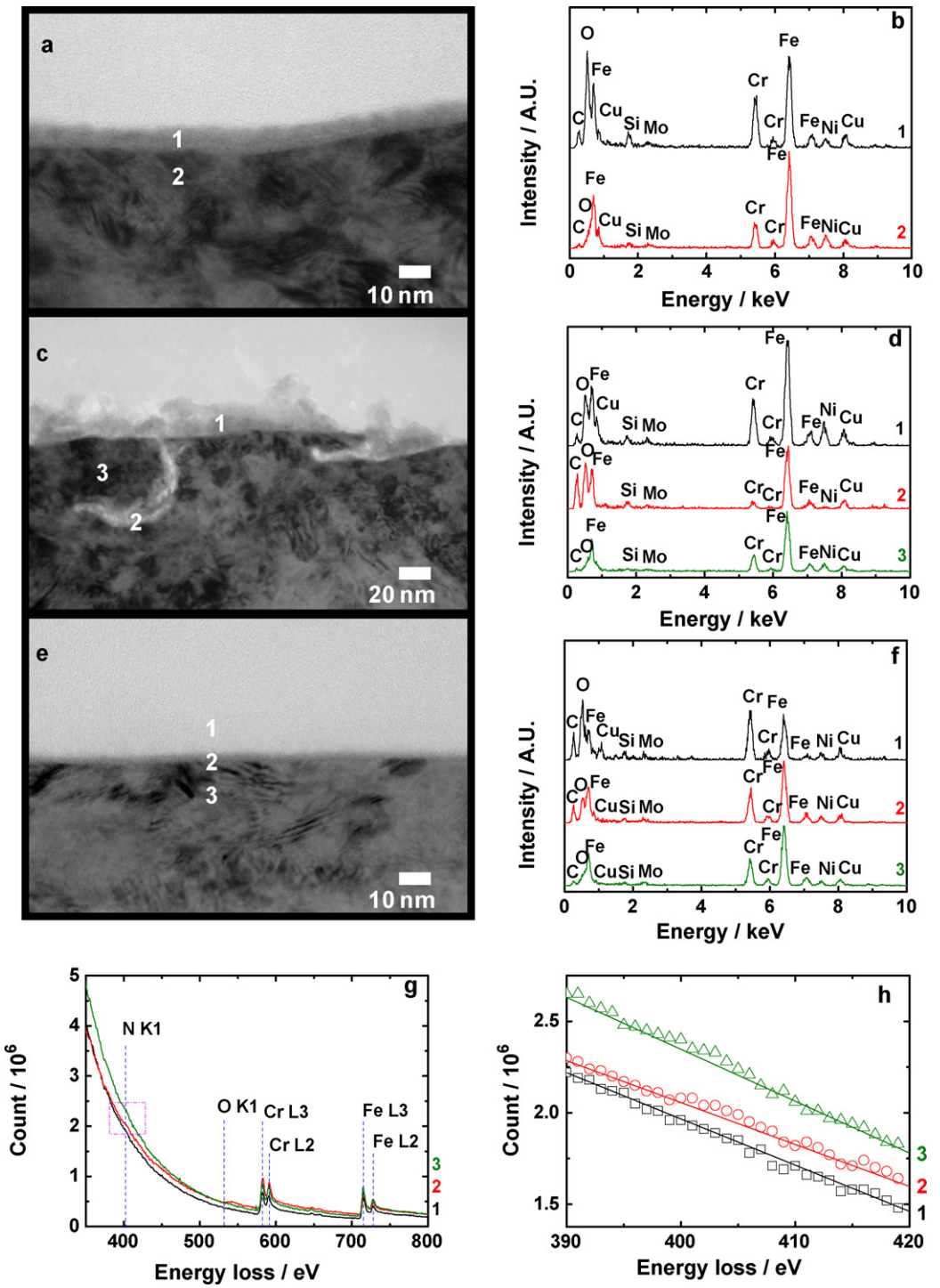

Fig. 6. TEM bright-field images of bipolar plate on the cathodic side after 1000 h of cell operation: (a) undamaged part for type 316L stainless steel and (b) the corresponding EDS spectrum; (c) damaged part for type 316L stainless steel and (d) the corresponding EDS spectrum; and (e) undamaged part for Ni-saving HNS, (f) the corresponding EDS spectrum, (g) the corresponding EELS spectrum, and (h) an enlarged view of (g) at the nitrogen K-edge.

corrosion products on the bipolar plates is likely to result in a great increase of the ICR and contamination of MEA, thereby affecting inferior cell performance.

The extensively operated Ni-saving HNS (cathodic side) was observed by TEM (Fig. 6e). The observed layer was thin and uniform, showing that the thickness of the passive layer is estimated to be 3–4 nm (Fig. 6e (point 1)). This indicates no significant change in the passive layer thickness before and after long-term cell operation. In the EDS spectra for the passive layer (Fig. 6f (point 1)), chromium intensity was stronger than the iron signal, meaning that the chromium oxide component composes the majority of the passive layer, which coincides with the XPS results (Fig. 4d). At the interface between the passive layer and the steel bulk (Fig. 6e (point 2) and f (point 2)), the intensity of oxygen element decreased abruptly. Unlike the passive layer, the iron intensity became stronger than chromium. Except for the passive layer, both steels exhibited the similar chemical states in bulk (Fig. 6d (point 3) and f (point 3)).

Although nitrogen, N, element is soluted in the bulk of the Ni-saving HNS, it was not detected in the EDS spectra because the content of nitrogen is not sufficient, approximately 1 mass%

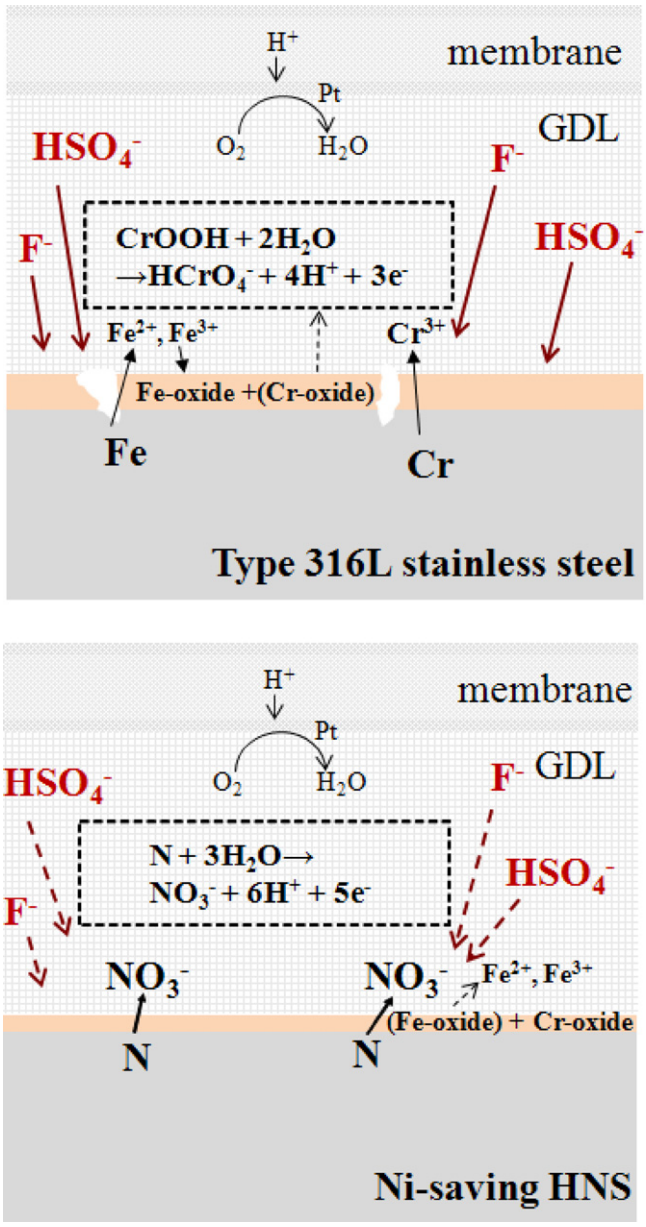

Fig. 7. Schematic of reactions at cathodic bipolar plate surface after 1000 h of cell operation.

(Table 1). Thus, the same points in Fig. 6e were analyzed by EELS (beam size 5 nm) to determine the behavior of the nitrogen in the Ni-saving HNS. Because the intensity of nitrogen was relatively weak (Fig. 6g), the squared part was magnified (Fig. 6h). In the passive layer, the nitrogen signal, which shows the characteristic signals at around 400–410 eV, was negligibly observed. This result demonstrates that the passive layer for the Ni-saving HNS is solely composed of chromium and iron oxide. When the interface of the passive layer and bulk was analyzed, the characteristic nitrogen signal was most strongly observed (Fig. 6h (point 2)). This indicates that nitrogen was concentrated at the interface between the passive layer and the based material bulk in the Ni-saving HNS.

Water is always formed at the cathodic side because of the oxygen reduction reaction. The generated water is drained through the flowing channel of the bipolar plate. Here, the soluted nitrogen of the steel reacts with the water on surface of the bipolar plate. The reaction gives rise to the formation of NO_3^- ions, accompanying the generation of H^+ ions that locally reduces the pH on the steel. Iron oxide is readily dissoluble at lower pH. Thus, the iron oxide constituting the passive layer is selectively dissolved, and the chromium-based oxide, thereby, is remained to protect the steel bulk as the passive layer. The process is summarized in Fig. 7.

According to the effect of the nitrogen in steel, the Ni-saving HNS could control the dissolution of iron and nickel under the PEMFC environment, compared with the type 316L stainless steel. As a result, the Ni-saving HNS bipolar plate employing cell exhibited superior cell performance, compared with the type 316L one. Slightly lower operation voltage can be improved by surface modification using nanosized TiN–SBR hybrid coating that is an available means to increase the operation voltage as high as graphite bipolar plate employing cell [23,24].

4. Conclusions

Commercial-type 316L stainless steel and the Ni-saving HNS were compared as bipolar plates for PEMFCs. The cell performance of the Ni-saving HNS bipolar plate employing cell was excellent, of which the voltage retention after 1000 h operation bares comparison with that of the graphite bipolar plate employing cell. The type 316L stainless steel, adopted on the cathodic side, was severely corroded after 1000 h of cell operation, as confirmed by SEM. However, corrosion products were not found for the Ni-saving HNS under the same condition. Chemical analyses of the bipolar plates after 1000 h of cell operation indicate that the presence of cations, such as Ni^{2+}, Fe^{2+}, and Cr^{3+} ions dissolved from the bipolar plate, were markedly reduced in MEA by employing the Ni-saving HNS, compared with that of the type 316L stainless steel. We found that, although the operation environment is similar for both the type 316L stainless steel and the Ni-saving HNS, different kinds of passive layer formation resulted in significant improvement in the operation voltage retention: iron oxide-based passive layer for the type 316L stainless steel and chromium oxide-based passive layer for the Ni-saving HNS. The chromium oxide-enriched passive layer was maintained throughout the cell operation for the Ni-saving HNS, which exhibited approximately 3 nm in thickness. The soluted nitrogen element in the Ni-saving HNS would be released to the interfacial solution and they induce protons by reacting with water on the passive layer, causing lowering of the local surface pH of the passive layer, and this, in turn, gives rise to the formation of the chromium oxide-enriched passive layer. Thus, the formed chromium oxide-based passive layer greatly reduced the dissolution of transition metal elements and prevented corrosion, so that it consequently improved the integrity of MEA, finally leading to excellent cell performance. Paying attention to the corrosion resistance of stainless steel bipolar plate, we suggested that the Ni-saving HNS is the most suitable alternative bipolar plate to graphite for PEMFC bipolar plates.

Appendix A. Supplementary data

Supplementary data associated with this article can be found, in the online version, at doi:10.1016/j.jpowsour.2011.11.033.

References

[1] K.R. Weisbrod, D. Prier II, N.E. Vanderbrogh, Progress report 1999, US DOE Hydrogen and Fuel Cell Program, 1999, p. 117.
[2] P.L. Hentall, J.B. Lakeman, G.O. Mepsted, P.L. Adcock, J.M. Moore, J. Power Sources 80 (1999) 235.
[3] S.-J. Lee, C.-H. Huang, Y.-P. Chen, C.-T.J. Hsu, Fuel Cell Sci. Technol. 2 (2005) 290.
[4] S. Joseph, J.C. McClure, P.J. Sebastian, J. Moreira, E. Valenzuela, J. Power Sources 177 (2008) 161.
[5] L. Ma, S. Warthesen, D.A. Shores, J. New Mater. Electrochem. Syst. 3 (2000) 221.
[6] D.P. Davies, P.L. Adcock, M. Turpin, S.J. Rowen, J. Appl. Electrochem. 30 (2000) 101.
[7] V.V. Nikam, R.G. Reddy, J. Power Sources 152 (2005) 146.

[8] H.-Y. Lee, S.-H. Lee, J.-H. Kim, M.-C. Kim, D.-M. Wee, Int. J. Hydrogen Energy 33 (2008) 4171.
[9] D.P. Davies, P.L. Adcock, M. Turpin, S.J. Rowen, J. Power Sources 86 (2000) 237.
[10] J. Wind, R. Spah, W. Kaiser, G. Bohm, J. Power Sources 105 (2002) 256.
[11] M.C. Li, C.L. Zeng, S.Z. Luo, J.N. Shen, H.C. Lin, C.N. Cao, Electrochim. Acta 48 (2003) 1735.
[12] H. Wang, M.A. Sweikart, J.A. Turner, J. Power Sources 115 (2003) 243.
[13] H. Wang, J.A. Turner, J. Power Sources 128 (2004) 193.
[14] H. Wang, G. Teeter, J. Turner, J. Electrochem. Soc. 152 (2005) B99.
[15] A.K. Iversen, Corros. Sci. 48 (2006) 1336.
[16] R. Tian, J. Sun, J. Wang, Rare Metals 25 (2006) 229.
[17] Y. Wang, D.O. Northwood, Int. J. Hydrogen Energy 32 (2007) 895.
[18] Y. Wang, D.O. Northwood, Electrochim. Acta 52 (2007) 6793.
[19] M. Kumagai, S.-T. Myung, S. Kuwata, R. Asaishi, H. Yashiro, Electrochim. Acta 53 (2008) 4205.
[20] H. Wang, J. Turner, J. Power Sources 180 (2008) 791.
[21] M. Kumagai, S.-T. Myung, R. Asaishi, Y. Katada, H. Yashiro, J. Power Sources 185 (2008) 815.
[22] Japan Automobile Research Institute, NEDO report, 2001.
[23] M. Kumagai, S.-T. Myung, R. Asaishi, Y.-K. Sun, H. Yashiro, Electrochim. Acta 54 (2008) 574.
[24] S.-T. Myung, S. Sakurada, M. Kumagai, H. Yashiro, Fuel Cells 10 (2010) 545.
[25] H. Tawfik, Y. Hung, D. Mahajan, J. Power Sources 163 (2007) 755.
[26] Sumitomo Metal Industries Ltd., NEDO report, 2002.
[27] H.P. Leckie, H.H. Uhlig, J. Electrochem. Soc. 133 (1966) 1262.
[28] H. Yashiro, D. Hirayasu, N. Kumagai, ISIJ Int. 42 (2002) 1477.
[29] E. Hamada, K. Yamada, M. Nagoshi, N. Makiishi, K. Sato, T. Ishii, K. Fukuda, S. Ishikawa, T. Ujiro, Corros. Sci. 52 (2010) 3851.